

Shoko Miyake · Shohei Yanagita · Tatsuo Yoshida

# Numerical studies on the structure of the cosmic ray electron halo in starburst galaxies

Received: date / Accepted: date

**Abstract** The structure of the cosmic ray electron halo of a starburst galaxy depends strongly on the nature of galactic wind and the configuration of the magnetic field. We have investigated these dependencies by solving numerically the propagation of electrons originating in starburst galaxies, most likely in supernova remnants. The calculations are made for several models for the galactic winds and for the configuration of the magnetic fields for comparison with observations. Our simulation of a quasi-radio halo reproduces both the extended structure of  $\sim 9$  kpc and the subtle hollow structure near the polar region of the radio halo that are observed in the starburst galaxy NGC 253. These findings suggest the existence of strong galactic wind in NGC 253.

**Keywords** cosmic ray halo · starburst galaxy · radio halo

**PACS** 95.30.Dr

## 1 Introduction

Cosmic ray electrons accelerated in galaxies propagate outward by diffusion and convection in galactic winds and eventually form an electron halo, the size of which depends on physical conditions such as the ambient magnetic field strength and strength of the galactic wind. The profile of nonthermal radio emission from the relativistic electrons reveals information on the nature of electron itself as well as information about the galactic wind from the starburst region and the configuration of the magnetic field. We have numerically investigated the structure of the cosmic ray electron halo of

starburst galaxies and the resultant radio halo to study the existence of the galactic winds and the configuration of the magnetic field. The calculation of the propagation of electrons is made by solving a coupled set of stochastic differential equations (SDE) which is equivalent to the so-called diffusion convection partial differential equation and which has been successfully applied to the study of the solar modulation phenomena of the galactic cosmic rays in the heliosphere. In this paper we shall use spherically symmetric and axially symmetric models for the galactic winds and for the configuration of the magnetic field [1,2]. We present details of the structure of electron halo and also the resultant structure of radio halo of starburst galaxies, with particular attention to NGC 253.

## 2 Numerical models

The SDE equivalent to the diffusion convection partial differential equation is written as

$$d\mathbf{X} = \mathbf{u}dt + \sqrt{2\kappa}d\mathbf{W}(t), \quad (1)$$

$$dP = -\frac{1}{3}P(\nabla \cdot \mathbf{u})dt - dP_{sync} - dP_{IC},$$

where  $\mathbf{X}$  and  $P$  are the position and the momentum of the particle,  $\mathbf{u}$  is the galactic wind velocity,  $P_{sync}$  and  $P_{IC}$  indicate the synchrotron and the inverse Compton momentum loss,  $\kappa$  is the diffusion coefficient, and  $d\mathbf{W}(t)$  is a Wiener process given by the Gaussian distribution.

We adopted

$$\begin{aligned} \kappa &= 100 \kappa_B \\ &= 3.3 \times 10^{24} \beta \left( \frac{P}{1 \text{ GeV}/c} \right) \left( \frac{B}{1 \mu\text{G}} \right)^{-1} [\text{cm}^2 \cdot \text{sec}^{-1}], \end{aligned} \quad (2)$$

$$\frac{dP_{sync}}{dt} = \frac{4}{3} \sigma_T \beta^{-1} \Gamma^2 \frac{B^2}{8\pi}, \quad (3)$$

$$\frac{dP_{IC}}{dt} = \frac{4}{3} \sigma_T \beta^{-1} \Gamma^2 U_{ph}, \quad (4)$$

S. Miyake  
 Faculty of Science, Ibaraki University, Mito 310-8512, Japan  
 JSPS Research Fellow  
 E-mail: 06nd408g@mcs.ibaraki.ac.jp

S. Yanagita  
 Faculty of Science, Ibaraki University, Mito 310-8512, Japan  
 Tel.: +81-29-228-8394  
 E-mail: yanagita@mx.ibaraki.ac.jp

T. Yoshida  
 Faculty of Science, Ibaraki University, Mito 310-8512, Japan  
 E-mail: yoshidat@mx.ibaraki.ac.jp

where  $\kappa_B$  is the Bohm diffusion coefficient,  $B$  is the magnetic field strength,  $\sigma_T$  is the Thomson cross section,  $\Gamma$  is the Lorentz factor of electrons, and  $U_{ph}$  is the energy density of the cosmic microwave background (CMB). Here we assume only CMB photons as the target photons for the inverse Compton process. In our simulation, particles start at a fixed final point and run backwards in time until they come to the galactic disk boundary which has a 7 kpc radius and 0.5 kpc thickness. The momentum spectrum  $f_{\mathbf{X}}(p)$  at arbitrary position  $\mathbf{X}$  is written as a convolution of the spectrum  $f_{\mathbf{X}_0}(p_0)$  at the galactic disk boundary with the normalized transition probability  $F(p_0, \mathbf{X}_0|p, \mathbf{X})$  obtained by our SDE method as

$$f_{\mathbf{X}}(p) = \int f_{\mathbf{X}_0}(p_0) F(p_0, \mathbf{X}_0|p, \mathbf{X}) dp_0. \quad (5)$$

Here the spectrum at the boundary is  $f_{\mathbf{X}_0}(p_0) \propto (m^2 c^4 + p_0^2 c^2)^{-1.6}/p_0$  which is assumed to be uniform at the galactic disk boundary.

The simple analytical model for the spherically symmetric and the axially symmetric galactic wind flow from a starburst galaxy are given by Chevalier and Clegg [1] and Zirakashvili and Voelk [2] respectively. We adopt their models for our simulations.

For the spherically symmetric model of Chevalier and Clegg, the analytical solutions in the galactic halo are given as

$$M^{2/(\gamma-1)} \left( \frac{\gamma-1+2/M^2}{1+\gamma} \right)^{(\gamma+1)/[2(\gamma-1)]} = \left( \frac{r}{R} \right)^2, \quad (6)$$

$$\rho u r^2 = \text{const}, \quad (7)$$

$$\rho u r^2 \left( \frac{1}{2} u^2 + \frac{\gamma}{\gamma-1} \frac{P}{\rho} \right) = \text{const}, \quad (8)$$

where  $M$  is the Mach number,  $r$  is the radial coordinate,  $R$  is radius of the wind base,  $\rho$  is the density,  $P$  is the pressure,  $u$  is the galactic wind velocity, and  $\gamma$  is the adiabatic index. We adopted  $R = 300$  pc,  $\gamma = 5/3$ , the mass loss rate  $\dot{M} = 3.9 M_\odot \text{ yr}^{-1}$ , and the energy production rate  $\dot{E} = 1.9 \times 10^{42} \text{ erg} \cdot \text{s}^{-1}$ . We also assume the magnetic field is frozen in the galactic wind flow, namely  $B(r) = (\rho(r)/\rho(R))^{2/3} B_0$ , where  $B_0$  is the  $B$  at  $r = R$ .  $B_0$  is assumed to be  $50 \mu\text{G}$ .

For the axially symmetric model of Zirakashvili and Voelk, the analytical solutions in the galactic halo are given as

$$u_r = u_\infty \cos \theta, \quad (9)$$

$$u_\theta = -(1 - \gamma^{-1}) u_\infty \sin \theta, \quad (10)$$

$$\rho(r, \theta) = \rho_g \sin^{-2 \frac{\gamma-1}{2\gamma-1}} \theta \left( \frac{r}{R_g} \right)^{-\frac{2\gamma}{2\gamma-1}}, \quad (11)$$

$$p(r, \theta) = \rho_g \sin^{\frac{2\gamma}{2\gamma-1}} \theta \left( \frac{r}{R_g} \right)^{-\frac{2\gamma}{2\gamma-1}}, \quad (12)$$

where  $u_r$  and  $u_\theta$  are the radial and latitudinal velocity component in cylindrical coordinates  $(r, \theta, z)$ ,  $\rho$  is the density,  $p$  is the pressure,  $u_\infty$  is the asymptotic velocity of the galactic wind,  $\gamma$  is the adiabatic index,  $R_g$  is the radius of the wind base, and  $\rho_g$  is the  $\rho$  at  $r = R_g$ . We adopted  $\gamma = 5/3$ ,  $R_g = 300$  pc and  $u_\infty = 900$  km/sec.

We used the following expression [2] for the magnetic field which has a similar  $r$ -dependence as  $p(r, \theta)$ ,

$$B = B_0 (\sin \theta)^{\frac{1}{\gamma-1}} \left( \gamma_m - \frac{\gamma^2}{2\gamma-1} \right) \left( \frac{r}{R_g} \right)^{-\frac{\gamma}{2\gamma-1}}, \quad (13)$$

where  $B_0$  is the magnetic field strength at the wind base and  $\gamma_m$  is the adiabatic index of an isotropic random magnetic field. We assumed  $B_0 = 50 \mu\text{G}$  and  $\gamma_m = 4/3$ .

### 3 Results

#### 3.1 Structure of cosmic ray electron halo

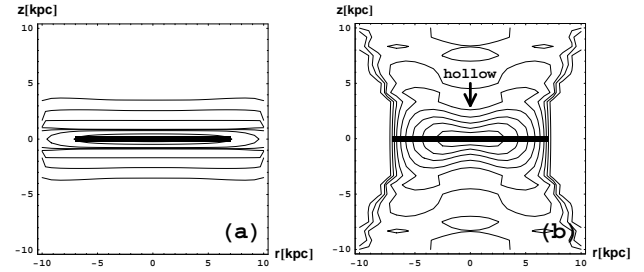


**Fig. 1** (a) Side view of 1 GeV electron intensities integrated along the line of sight in the spherically symmetric model. The black rectangle indicates the galactic disk boundary. The peak intensity is normalized to 1.0. Contours indicate  $10^{-6}$ ,  $10^{-5}$ ,  $10^{-4}$ ,  $10^{-3}$ , 0.01, 0.1, 0.5, and 0.8.; (b) Same as (a) in the axially symmetric model. Contours indicate 0.1, 0.2, 0.3, ..., 0.8, and 0.9.

Fig. 1 shows side views of the 1 GeV electron intensities integrated along the line of sight in the spherically symmetric and the axially symmetric models. The filled rectangle at the center indicates the side view of the galactic disk. We can see in Fig. 1 there is a big difference in the structure and the size of the resultant electron halo of the two models for symmetry. One reason for this difference comes from the difference in the distribution of the source position of electrons on the galactic disk boundary. In the axially symmetric model electrons may come from almost any point on the galactic disk boundary, however, in spherical symmetric model almost all electrons should originate near the galactic center where the magnetic field intensity is high and electrons suffer severe energy loss. The spherical symmetry model clearly does not reproduce the observed radio halo of NGC 253 [3]. We discuss below only the results for axially symmetric models, because in many actual cases the

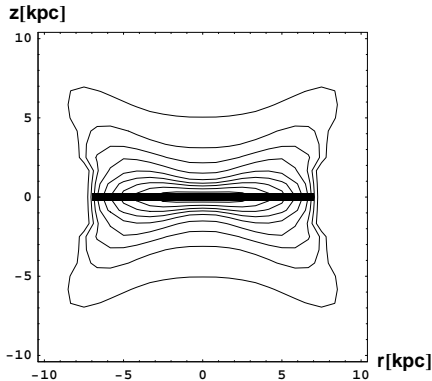


**Fig. 2** Side view of electron intensities integrated along the line of sight in the axially symmetric model for 10 GeV electrons. The black rectangle indicates the galactic disk boundary. The peak intensity is normalized to 1.0. Contours indicate 0.1, 0.2, 0.3,..., 0.8, and 0.9.

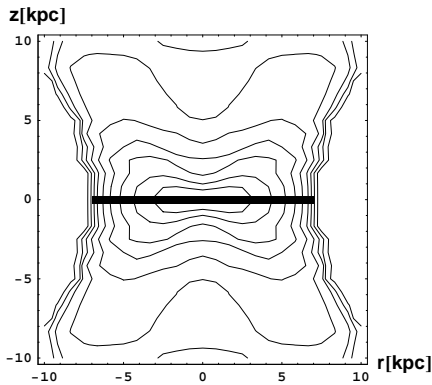


**Fig. 3** Side view of 1 GeV electron intensities integrated along the line of sight in the axially symmetric model for a  $B_0$  of  $5 \mu\text{G}$ . The black rectangle indicates the galactic disk boundary. The peak intensity is normalized to 1.0. Contours indicate 0.1, 0.2, 0.3,..., 0.8, and 0.9.

starburst region has an ellipsoidal shape or a disk geometry [2].

Propagation of electrons is governed by the diffusion process and convection in the expanding galactic wind and the associated energy loss processes. The diffusion process depends on the electron energy, however the convection does not. The adiabatic loss is proportional to the electron energy, and the other energy loss processes are proportional to the square of electron energy. The synchrotron energy loss is larger than the inverse Compton energy loss, because  $B^2/8\pi \gg U_{ph}$ . Accordingly the resultant structure depends on the energy of the electrons as we will see below. Fig. 2 shows a side view of the electron intensities integrated along the line of sight in the axially symmetric model for 10 GeV electrons. The contours in Fig. 2 were drawn with the same steps in Fig. 1.b for easier comparison. The higher the electron energy, the smaller the size of the halo, due to the shorter

synchrotron cooling time. For the axially symmetric model the TeV electron halo is not formed, because the synchrotron cooling time of TeV electrons is  $\sim 5 \times 10^3$  years, and the diffusion length is only about 1 pc. This is consistent with the H.E.S.S. result of TeV  $\gamma$ -ray observation of NGC 253 [4]. The synchrotron energy loss is proportional to the square of magnetic field strength, therefore the weaker the magnetic field strength, the larger the size of the halo. Fig. 3 shows a side view of the 1 GeV electron intensities integrated along the line of sight in the axially symmetric model for a  $B_0$  of  $5 \mu\text{G}$ . The size of the halo shown in Fig. 3 is much larger than that shown in Fig. 1b as expected.

A slight hollow structure near the polar region in electron halo is visible in Fig. 1b and Fig. 3 for 1 GeV electrons and in Fig. 2 for 10 GeV electrons. This structure comes from the  $r$  dependence of energy loss in cylindrical coordinates  $(r, \theta, z)$ . Fig. 4a shows the mean total energy loss of 1 GeV electrons at  $z = 5 \text{ kpc}$  as a function of  $r$ . The energy loss peaks near the polar region, as the energy loss is dominated by the adiabatic loss, as shown in Fig. 4b, by the convection due to the galactic wind and as the wind velocity is higher in polar region as shown by Eq.9. Fig. 4b shows the  $r$  dependence of the fraction of the energy loss shown in Fig. 4a for the three processes, adiabatic, synchrotron, and inverse Compton. The slight hollow structure for 10 GeV electrons seen in Fig. 2 comes from the dominance of synchrotron loss over the other two energy loss mechanisms. (Due to page limitations we cannot present a similar figure to Fig. 4 in this paper.) The rate of synchrotron energy loss is proportional to the square both of energy and magnetic field strength. The magnetic field strength is higher in the polar region as shown by Eq.13. Electrons which arrive at the polar region originate from near the galactic center where they suffer severe energy loss at the start of their journey.

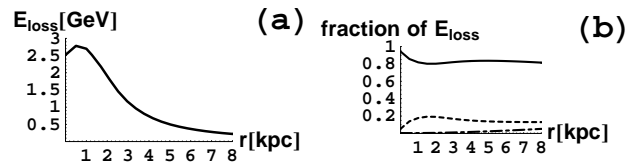


**Fig. 4** (a) Mean energy loss of electrons arriving at  $z = 5 \text{ kpc}$  with an energy of 1 GeV as a function of  $r$ . (b) The fraction of energy loss for three processes corresponding to the mean energy loss shown in (a). The solid line indicates the adiabatic energy loss. The dotted line indicates the synchrotron radiation loss. The dot-dash line indicates the inverse Compton radiation loss.

The differential electron energy spectrum varies with position due to the variation of the total energy loss. Fig. 5 shows the simulated electron energy spectra at several selected positions. The modulated spectrum shifts from the spectrum at the galactic disk boundary to the low energy region without changing shape while the energy loss is dominated by the adiabatic loss, namely  $d\log E \propto \text{const}$ , where

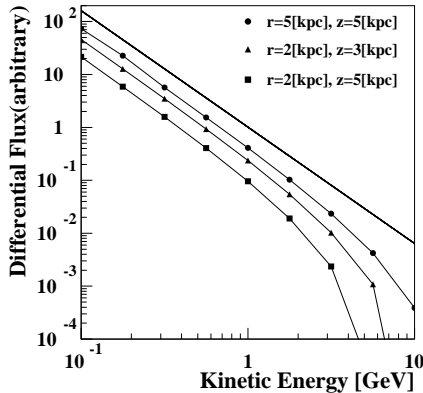


**Fig. 5** Simulated electron energy spectra at several selected positions. The solid lines indicate the energy spectra in the electron halo. The dotted line indicates the energy spectrum in the galactic disk.

$E$  is the electron energy. But the spectrum steepens in the high energy region due to the synchrotron energy loss. The bending point of the spectrum appears as expected at the electron energy where the adiabatic loss rate equals to the synchrotron energy loss rate [5].

### 3.2 Comparison with observation

NGC 253 is a nearby edge-on starburst galaxy at a distance of 2.5 Mpc. The galaxy has two spiral arms, and a bar of projected length 7 kpc. It has an extended nonthermal radio halo of  $\sim 9$  kpc. It has also extended X-ray halo, possibly related to the galactic wind.

Fig. 6 shows side view of the 1 GeV electron intensities multiplied by  $B^2$  and integrated along the line of sight in the axially symmetric model. As the power of synchrotron radiation is proportional to electron intensity times the square of magnetic field strength, Fig. 6 may mimic the radio intensity profile.

Our result for the quasi-radio intensity profile qualitatively reproduces the observed large radio halo of  $\sim 9$  kpc. The contours in Fig. 6 are drawn with steps proportional to the steps in Fig. 2 of Carilli et al. [3] for ease of comparison of the results of our simulations with the observed radio halo. Looking closer at the observed halo, shown in Fig. 2 of Carilli et al. [3], we can recognize a slight hollow near the polar region and prominence far above the disk. Our quasi-radio halo reproduce these two features as seen in Fig. 6. The hollow structure comes from adiabatic cooling of electrons by the higher velocity galactic wind near the polar region as shown in Fig. 1b. Our results suggest the existence of a strong galactic wind in NGC 253. In our simulation, the cosmic ray sources are assumed to be distributed uniformly in the galactic disk. The nature of galactic winds and magnetic fields in starburst galaxies will be revealed by further simulation experiments based on models which take into account a more realistic distribution of cosmic ray sources in galaxies.

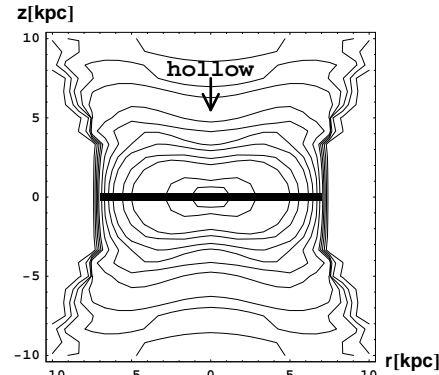


**Fig. 6** Side view of electron (1 GeV) intensities times  $B^2$  integrated along the line of sight in the axially symmetric model. The black rectangle indicates the galactic disk boundary. The peak value is normalized to 1.0. Contours indicate 0.005, 0.01, 0.015, 0.02, 0.025, 0.0375, 0.05, 0.0625, 0.075, 0.1, 0.125, 0.25, and 0.5.

## 4 Conclusions

We have examined numerically the structure of the cosmic ray electron halo of starburst galaxies. We confirmed that the formation of electron halo extending to  $\sim 9$  kpc from galaxies is possible for the axially symmetric model of the galactic wind flow and the magnetic field configuration. Furthermore, a subtle hollow structure of radio halo near the polar region observed in NGC 253 was reproduced. This structure may come from large energy loss near at the polar region by either the adiabatic energy loss due to strong galactic wind or the synchrotron energy loss due to relatively strong magnetic field there. These findings suggest the existence of strong galactic wind in NGC 253.

**Acknowledgements** We are grateful to Phil Edwards for careful reading of the manuscript and important suggestions. S. Miyake is supported by a JSPS Research Fellowship.

## References

1. Chevalier, R. A., Clegg, A. W.: Wind from a starburst galaxy nucleus. *Nature* **317**, 44–45 (1985)
2. Zirakashvili, V. N., Voelk, H. J.: Simple model of the outflow from starburst galaxies: Application to radio observations. *Astrophys. J.* **636**, 140–148, (2006)
3. Carilli, C. L., Holdaway, M. A., Ho, P. T. P., De Pree, C. G.: Discovery of synchrotron-emitting halo around NGC253. *Astrophys. J. (Letters)* **399**, L59–L62 (1992)
4. Aharonian, F., Akhperjanian, A. G., Bazer-Bachi, A. R., et al. (HESS Collaboration): A search for very high energy  $\gamma$ -ray emission from the starburst galaxy NGC 253 with HESS. *Astron. Astrophys.* **442**, 177–183, (2005)
5. Lerche, I., Schlickeiser, R.: Dynamical or static radio halo—Is there a galactic wind? *Astrophys. Letters* **22**, 161–163, (1981)